observations. However, as Lense-Thirring precession is prograde, a beat between a pulsar beam and a precessing orbit would produce a sideband below, rather than the observed sideband above, the pulsar frequency. Another resonance, perhaps at the radius where the general relativistic vertical epicyclic frequency matches $\nu_{\rm spin}$, might be considered as an explanation of this phenomenon. □

Received 19 March; accepted 25 May 2003; doi:10.1038/nature01754.

1. Svartsman, V. F. Halos around black holes. *Sov. Astron* **15,** 377–384 (1971).
2. Van der Klis, M. *et al.* Intensity dependent quasi-periodic oscillations in the X-ray flux of GX 5-1. *Nature* **316,** 225–230 (1985).
3. Van der Klis, M. Millisecond oscillations in X-ray binaries. *Annu. Rev. Astron. Astrophys.* **38,** 717–760 (2000).
4. Alpar, M. A. & Shaham, J. Is GX. 5-1. a millisecond pulsar? *Nature* **316,** 239–241 (1985).
5. Lamb, F. K., Shibazaki, N., Alpar, M. A. & Shaham, J. Quasi-periodic oscillations in bright galactic-bulge X-ray sources. *Nature* **317,** 681–687 (1985).
6. Miller, C. M., Lamb, F. K. & Psaltis, D. Sonic-point model of kilohertz quasi-periodic brightness oscillations in low-mass X-ray binaries. *Astrophys. J.* **508,** 791–830 (1998).
7. Stella, L. & Vietri, M. KHz quasi-periodic oscillations in low-mass X-ray binaries as probes of general relativity in the strong-field regime. *Phys. Rev. Lett.* **82,** 17–20 (1999).
8. Titarchuk, L., Lapidus, I. & Muslimov, A. Mechanisms for high-frequency quasi-periodic oscillations in neutron stars and black hole binaries. *Astrophys. J.* **449,** 315–328 (1998).
9. Kluźniak, W. & Abramowicz, M. A. The physics of kHz QPOs—strong gravity's coupled anharmonic oscillators. *Astrophys. J. Lett.* (submitted); preprint at ⟨http://xxx.lanl.gov/astro-ph/0105057⟩ (2001).
10. Psaltis, D. & Norman, C. On the origin of quasi-periodic oscillations and broad-band noise in accreting neutron stars and black holes. *Astrophys. J.* (submitted); preprint at ⟨http://xxx.lanl.gov/astro-ph/0001391⟩ (2000).
11. Strohmayer, T. & Bildsten, L. New views of thermonuclear bursts. In *Compact Stellar X-ray Sources* (eds Lewin, W. H. G. & van der Klis, M.) (Cambridge Univ. Press, in the press); preprint at ⟨http://xxx.lanl.gov/astro-ph/0301544⟩ (2003).
12. Strohmayer, T. E. *et al.* Millisecond X-ray variability from an accreting neutron star system. *Astrophys. J.* **469,** L9–L12 (1996).
13. Cui, W. On the disappearance of kilohertz quasi-periodic oscillations at high mass accretion rate in low-mass X-ray binaries. *Astrophys. J.* **534,** L31–L34 (2000).
14. Campana, S. Kilohertz quasi-periodic oscillations in low-mass X-ray binary sources and their relation to the neutron star magnetic field. *Astrophys. J.* **534,** L79–L82 (2000).
15. Muno, M. P., Özel, F. & Chakrabarty, D. The amplitude evolution and harmonic content of millisecond oscillations in thermonuclear X-ray bursts. *Astrophys. J.* **581,** 550–561 (2002).
16. Van der Klis, M., Wijnands, R. A. D., Horne, K. & Chen, W. Kilohertz quasi-periodic oscillation peak separation is not constant in Scorpius X-1. *Astrophys. J.* **481,** L97–L101 (1997).
17. Méndez, M. *et al.* Kilohertz quasi-periodic oscillation peak separation is not constant in the atoll source 4U 1608-52. *Astrophys. J.* **505,** L23–L26 (1998).
18. Méndez, M., van der Klis, M. & van Paradijs, J. Difference frequency of kilohertz QPOs not equal to half the burst oscillation frequency in 4U 1636-53. *Astrophys. J.* **506,** L117–L119 (1998).
19. Jonker, P. G., Méndez, M. & van der Klis, M. Kilohertz quasi-periodic oscillations difference frequency exceeds inferred spin frequency in 4U 1636-53. *Mon. Not. R. Astron. Soc.* **336,** L1–L5 (2002).
20. Lamb, F. K. & Miller, M. C. Changing frequency separation of kilohertz quasi-periodic oscillations in the sonic-point beat-frequency model. *Astrophys. J.* **554,** 1210–1215 (2001).
21. Wijnands, R. & van der Klis, M. A millisecond pulsar in an X-ray binary system. *Nature* **394,** 344–346 (1998).
22. Markwardt, C. B., Miller, J. M. & Wijnands, R. SAX J1808.4-3658. *IAU Circ. No. 7993* (2002).
23. Chakrabarty, D. *et al.* Nuclear-powered millisecond pulsars and the maximum spin frequency of neutron stars. *Nature* (this issue).
24. Shibazaki, N. & Lamb, F. K. Power spectra of quasi-periodic oscillations in luminous X-ray stars. *Astrophys. J.* **318,** 767–785 (1987).
25. Psaltis, D. Models of quasi-periodic variability in neutron stars and black holes. *Adv. Space Res.* **555,** 786–800 (2001).
26. Stella, L. in *X-ray Astronomy: Stellar Endpoints, AGN, and the Diffuse X-ray Backgroud* (eds White, N. E., Malaguti, G. & Palumbo, G. G. C.) 365–375 (AIP Conference Proceedings Vol. 599, Melville, New York, 2001).
27. van der Klis, M. in *XEUS–Studying the Evolution of the Hot Universe* (eds Hasinger, G., Boller, Th. & Parmar, A.) 354–362 (MPE Report 281, 2002).
28. Abramowicz, M. A., Karas, V., Kluźniak, W., Lee, W. H. & Rebusco, P. Non-linear resonance in nearly geodesic motion in low-mass X-ray binaries. *Publ. Astron. Soc. Jpn* **55,** 467–471 (2003).
29. Jonker, P. G., Méndez, M. & van der Klis, M. Discovery of a new, third kilohertz quasi-periodic oscillations in 4U 1608-52, 4U 1728-34, and 4U 1636-53: Sidebands to the lower kilohertz quasi-periodic oscillation? *Astrophys. J.* **540,** L29–L32 (2000).
30. Stella, L. & Vietri, M. Lense-Thirring precession and quasi-periodic oscillations in low-mass X-ray binaries. *Astrophys. J.* **492,** L59–L62 (1998).

Acknowledgements We thank J. Swank and E. Smith for their efforts in scheduling our RXTE observations of SAX J1808.4−3658, and D. Psaltis for discussions. M.v.d.K. was supported by NWO.

Competing interests statement The authors declare that they have no competing financial interests.

Correspondence and requests for materials should be addressed to R.W. (radw@st-andrews.ac.uk.).

Creation of ultracold molecules from a Fermi gas of atoms

Cindy A. Regal*, Christopher Ticknor*, John L. Bohn* & Deborah S. Jin†

** JILA, National Institute of Standards and Technology and Department of Physics, University of Colorado, Boulder, Colorado 80309-0440, USA*
† Quantum Physics Division, National Institute of Standards and Technology, Boulder, Colorado 80309-0440, USA

Following the realization of Bose–Einstein condensates in atomic gases, an experimental challenge is the production of molecular gases in the quantum regime. A promising approach is to create the molecular gas directly from an ultracold atomic gas; for example, bosonic atoms in a Bose-Einstein condensate have been coupled to electronic ground-state molecules through photoassociation[1] or a magnetic field Feshbach resonance[2]. The availability of atomic Fermi gases offers the prospect of coupling fermionic atoms to bosonic molecules, thus altering the quantum statistics of the system. Such a coupling would be closely related to the pairing mechanism in a fermionic superfluid, predicted to occur near a Feshbach resonance[3,4]. Here we report the creation and quantitative characterization of ultracold $^{40}K_2$ molecules. Starting with a quantum degenerate Fermi gas of atoms at a temperature of less than 150 nK, we scan the system over a Feshbach resonance to create adiabatically more than 250,000 trapped molecules; these can be converted back to atoms by reversing the scan. The small binding energy of the molecules is controlled by detuning the magnetic field away from the Feshbach resonance, and can be varied over a wide range. We directly detect these weakly bound molecules through their radio-frequency photodissociation spectra; these probe the molecular wavefunction, and yield binding energies that are consistent with theory.

Feshbach resonances occur when the collision energy of two free atoms coincides with that of a quasi-bound molecular state[5–7]. By varying the strength of an external magnetic field, experimenters can tune the relative atom–molecule energy through the Zeeman effect. This enables control over the strength of cold atom interactions, characterized by the *s*-wave scattering length a, as well as whether these interactions are effectively repulsive ($a > 0$) or attractive ($a < 0$). These resonances have been used to tune the interaction strength between atoms for both Bose and Fermi gases[8–16].

Another possible use of a Feshbach resonance is to controllably convert atoms into molecules. The energy of the molecular state associated with the Feshbach resonance coincides with the free atom threshold at the resonance peak, and the binding energy of the molecule varies smoothly with magnetic field on the repulsive side of the resonance ($a > 0$). Thus, one would expect that atoms could be coupled to molecules by ramping the detuning from the resonance using a time-dependent magnetic field[17–19]. For example, ramping the magnetic field through a Feshbach resonance resulted in large losses in a ^{23}Na Bose–Einstein condensate (BEC)[20]. Further, coherent oscillations between atoms and molecules in a BEC were observed following magnetic field pulses on the repulsive side of a ^{85}Rb Feshbach resonance[2]. Here we report the efficient creation of bosonic molecules from fermionic ^{40}K atoms using a magnetic field ramp across a Feshbach resonance. We present clear evidence of diatomic molecule formation through direct, spectroscopic detection of these molecules.

The experiments reported here use previously developed techniques for cooling and spin state manipulation of ^{40}K (refs 10, 15, 21). Because of the quantum statistics of fermions, a mixture of two components—for example, atoms in different internal spin states—

is required to have *s*-wave interactions in the ultracold gas. With a total atomic spin $f = 9/2$ in its lowest hyperfine ground state, ^{40}K has ten available Zeeman spin-states m_f, where m_f is the spin projection quantum number.

Mixtures of atoms in two of these spin states are used in evaporative cooling of the gas, first in a magnetic trap and then in a far-off resonance optical dipole trap. The optical trapping potential has the distinct ability to trap atoms in any spin state as well as any molecules created from these atoms. For these experiments, the optical trap is characterized by radial frequencies ranging from $\nu_r = 215$ to 276 Hz, with the trap aspect ratio, ν_r/ν_z, fixed at 70 ± 20. The temperature T of these two-component gases, measured in units of the Fermi temperature T_F, ranges from $T/T_F = 0.13$ to 0.33. This degree of quantum degeneracy is near the lowest ever demonstrated in a Fermi gas of atoms[14,15].

Experiments are initiated by preparing atoms in a nearly equal, incoherent mixture of the $m_f = -5/2$ and $m_f = -9/2$ spin states. With these states, we access a previously reported Feshbach resonance located at a magnetic field of 224.21 ± 0.05 G (Fig. 1b)[15]. A time-dependent current through an auxiliary coil provides magnetic field ramps near the resonance. Starting from a magnetic field of 227.81 G, the field is ramped at a rate of 40 μs G^{-1} across the resonance to various final values. The number of atoms remaining following the ramp is determined from an absorption image of the cloud (at ~4 G) after expansion from the optical trap. As the light used for these images is resonant with the atomic transition, but not with any molecular transitions, we selectively detect only the atoms. In Fig. 1a we present the observed atom number as a function of the final magnetic field value of the ramp. We find that the atoms disappear abruptly at the Feshbach resonance peak.

We also investigate the atom loss as a function of the rate of the magnetic field sweep. Figure 2 illustrates the result of linear magnetic field ramps across the Feshbach resonance from 228.25 G to 216.15 G. For our fastest sweeps there is no observable effect upon the atoms, whereas significant atom number loss is observed for slower sweeps. For our slowest sweeps, we find that the number of atoms lost saturates at 50%. This loss cannot be explained by inelastic loss, because the atoms vanish at least two orders of magnitude more quickly than expected from previously measured inelastic collision rates at a resonance[13]. When we reverse the process by applying an additional magnetic field ramp across the Feshbach resonance in the opposite direction, we observe a return of nearly all the 'lost' atoms (Fig. 2). This is consistent with the lost atom number corresponding to trapped molecules. Further, we can measure the lifetime τ of the molecules by varying the time before conversion back to atoms. We find that $\tau \approx 1$ ms, presumably owing to vibrational quenching of these highly vibrationally excited molecules[22].

Surprisingly, the number of molecules produced is very large, despite the fact that the Fermi gas is not described by a single wavefunction as is a BEC. In fact, the number of molecules is sufficiently large that the temperature of an initial atomic gas at $T/T_F = 0.13$ is three times lower than the molecular Bose–Einstein condensation temperature T_c in the optical trap. Our calculation of T_c assumes that these weakly bound molecules have a polarizability twice that of a single atom, and hence are subject to the same trapping frequency as the atoms[23]. Future experiments could probe the distribution of energies in the ultracold molecular gas.

Using radio-frequency (r.f.) spectroscopy we directly probe the ultracold molecules. First, we create the molecules with a 40 μs G^{-1} magnetic field ramp. This ramp starts at 227.81 G, and ends at various final magnetic field values, B_{hold}, below the resonance. At B_{hold}, a 13-μs r.f. pulse is applied to the cloud; the radio frequency is

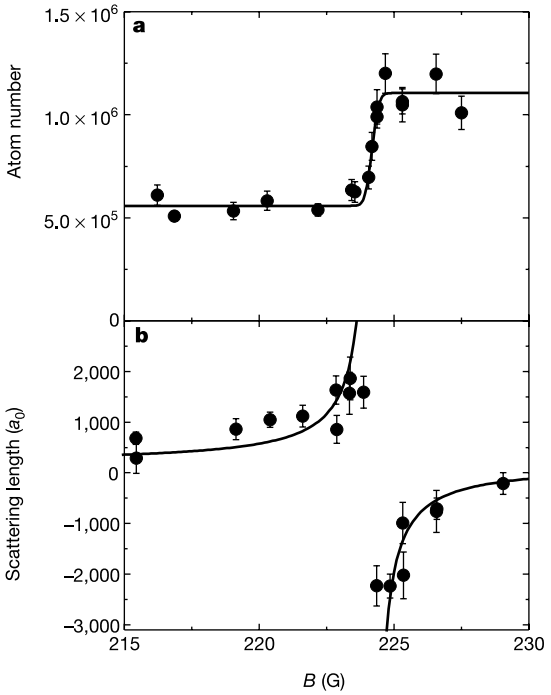

Figure 1 Atom loss following magnetic field ramps across a Feshbach resonance in ^{40}K. **a**, Number of $m_f = -5/2$ and $m_f = -9/2$ atoms as a function of the final magnetic field value B of a 40 μs G^{-1} ramp that starts at 227.81 G. The atom cloud is initially at $T/T_F = 0.21$ with $n_{pk} = 2.1 \times 10^{13}$ cm^{-3}, where n_{pk} is the peak atomic density of the two-component cloud. The relative number of $m_f = -9/2$ and $m_f = -5/2$ atoms remains approximately equal throughout the experiment. The data are fitted to an error function. The resulting gaussian width of the transition region is 0.21 ± 0.07 G, and the transition position is $B_0 = 224.18 \pm 0.05$ G. **b**, For comparison, we plot a previous measurement of the Feshbach resonance[15]. The resonance peak was found to be at 224.21 ± 0.05 G.

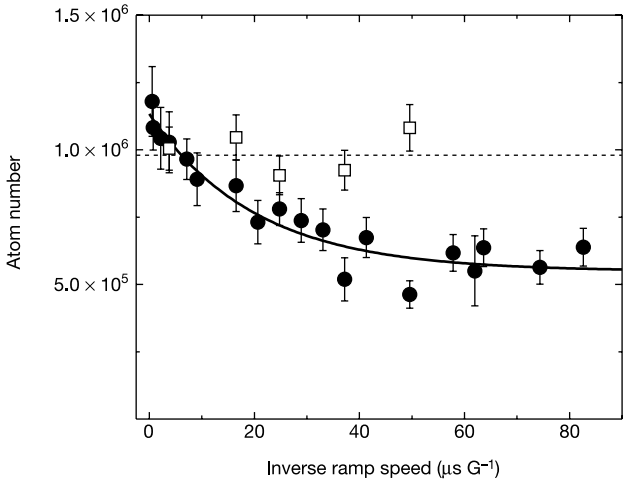

Figure 2 Dependence of atom loss on the magnetic field ramp rate through the Feshbach resonance. Filled circles, atom number following a magnetic field ramp across the Feshbach resonance from high to low field. The data are taken with $T/T_F = 0.33$ and $n_{pk} = 1.4 \times 10^{13}$ cm^{-3}. In accordance with a Landau–Zener model, we fit the data to an exponential (solid line); we find that the decay constant is 20 ± 6 μs G^{-1}. Data taken at $T/T_F = 0.13$ and $n_{pk} = 9 \times 10^{12}$ cm^{-3} behave similarly. Open squares, data for which the magnetic field was first ramped downward at a rate of 40 μs G^{-1} across the resonance to create molecules, and then ramped back above the Feshbach resonance at varying rates to again create free atoms. The dashed line is the average of the square points.

chosen so that the photon energy is near the energy splitting between the $m_f = -5/2$ and $m_f = -7/2$ atom states. The resulting population in the $m_f = -7/2$ state, which is initially unoccupied, is then probed selectively either by separating the spin states spatially using a strong magnetic field gradient during free expansion (Stern–Gerlach imaging), or by leaving the magnetic field high (215 G) and taking advantage of nonlinear Zeeman shifts.

Figure 3a shows a sample r.f. spectrum at $B_{hold} = 222.49$ G; the resulting number of atoms in the $m_f = -7/2$ state is plotted as a function of the frequency of the r.f. pulse. We observe two distinct features in the spectrum. The sharp, symmetric peak is very near the expected $m_f = -5/2$ to $m_f = -7/2$ transition frequency for free atoms, ν_{atom}. With the Stern–Gerlach imaging we see that the total number of $m_f = -5/2$ and $m_f = -7/2$ atoms is constant, consistent with transfer between these two atom states. The width of this line is defined by the Fourier width of the applied r.f. pulse. Nearby is a broader, asymmetric peak shifted lower in frequency. Here we find that the total number of observed atoms ($m_f = -5/2 + m_f = -7/2$) after the r.f. pulse actually increases (Fig. 4). Also, the resulting $m_f = -7/2$ gas in this region has a significantly increased kinetic energy, which grows linearly for larger frequency shifts from the atom peak (Fig. 3b).

The asymmetric peak can be interpreted as the dissociation of molecules into free $m_f = -7/2$ and $m_f = -9/2$ atoms. Because the applied r.f. pulse stimulates a transition to a lower energy Zeeman state, we expect $h\nu_{rf} = h\nu_{atom} - E_{binding} - \Delta E$, where h is Planck's constant, $E_{binding}$ is the binding energy of the molecule, and we have ignored mean-field interaction energy shifts. The remaining energy, ΔE, must be imparted to the dissociating atom pair as kinetic energy. Further, the observed lineshape of the asymmetric peak should depend on the Franck-Condon factor, which gives the overlap of the molecular wavefunction with the wavefunction of the free atom pair.

We have calculated this multichannel Franck–Condon overlap as a function of energy. The resulting transition rate, convolved with the frequency width of the applied r.f. and scaled vertically, is shown as the solid line in Fig. 3a. The agreement between theory and experiment for the dissociation spectrum is quite good. This well-resolved spectrum provides much information about the molecular wavefunction. For example, the mean interatomic separation within each molecule at this magnetic field is extremely large, 170 a_0, where a_0 is the Bohr radius.

In Fig. 5 we plot the magnetic field dependence of the frequency shift $\Delta\nu$ between the atom line and the threshold of the molecular spectrum, which should correspond to the molecular binding energy. Although this could in principle be obtained directly from the transfer spectrum (Fig. 3a), the appearance of the threshold in

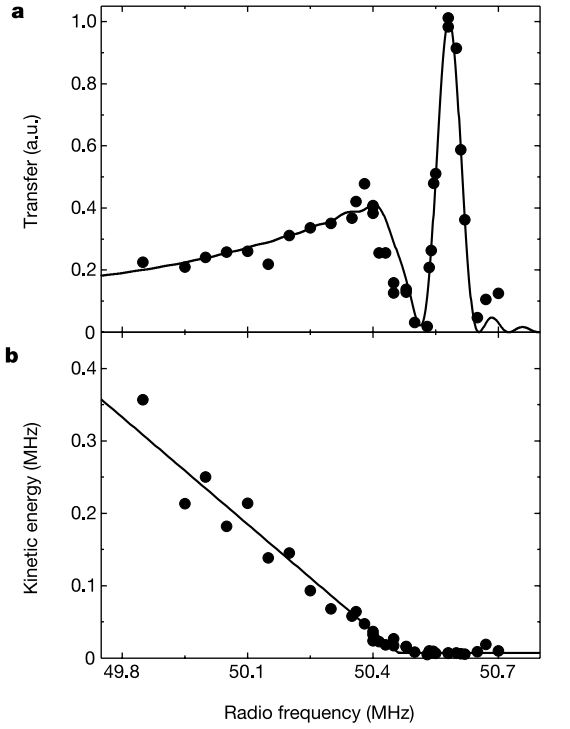

Figure 3 Photodissociation spectrum of ultracold molecules, and resulting energy per atom. **a**, Dissociation spectrum at $B_{hold} = 222.49$ G, with an original atom cloud containing $N = 1.4 \times 10^6$ atoms at $T/T_F = 0.26$, where N is the total number of atoms in the two-component cloud. The relative number of $m_f = -7/2$ atoms after an applied r.f. pulse is plotted versus radio frequency. The solid line is the weighted sum of the atomic transition line and the calculated dissociation spectrum, both convolved with the frequency width of the r.f. pulse. **b**, Resulting kinetic energy per $m_f = -7/2$ atom. Two separate linear fits are applied to the data to determine the threshold position. The slope beyond threshold is 0.49 ± 0.03; this indicates that the atom pair ($m_f = -7/2 + m_f = -9/2$) receives the additional energy ΔE beyond the binding energy when the molecule is dissociated.

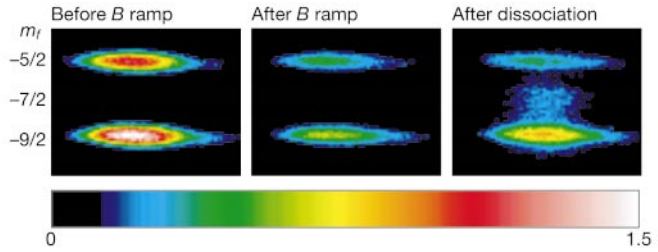

Figure 4 Absorption images of the quantum gas using a Stern–Gerlach technique. We start with ultracold fermionic atoms in the $m_f = -5/2$ and $m_f = -9/2$ states of ^{40}K. A magnetic field ramp through the Feshbach resonance causes 50% atom loss, owing to adiabatic conversion of atoms to diatomic molecules. To directly detect these bosonic molecules we apply an r.f. photodissociation pulse; the dissociated molecules then appear in the $m_f = -7/2$ and $m_f = -9/2$ atom states. The shaded bar indicates the optical depth.

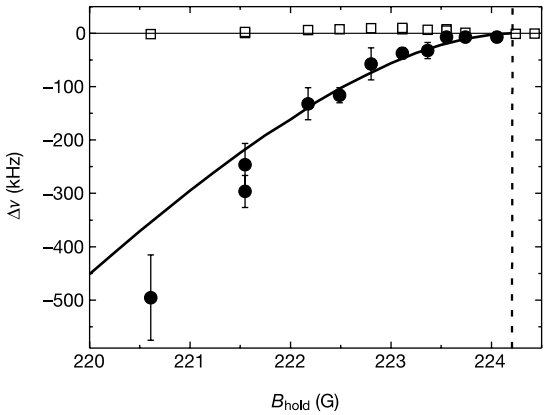

Figure 5 Binding energy of the molecules. The frequency shift $\Delta\nu$ from the expected $m_f = -5/2$ to $m_f = -7/2$ transition is plotted versus magnetic field for the atoms (open squares) and the molecules (filled circles). The typical atom cloud before molecule creation is characterized by $T/T_F = 0.14$ and $N = 7 \times 10^5$. The dashed line indicates the Feshbach resonance position. The solid line is a calculation of the binding energy of the molecules as a function of detuning from the resonance.

the energy of the $m_f = -7/2$ cloud is more clear (Fig. 3b). We compare the position of this energy threshold to the expected atom–atom transition frequency ν_{atom} based upon a calibration of the magnetic field strength. The data are consistent with a theoretical calculation of the binding energy (solid line) based upon a full coupled channels calculation with no free parameters.

This agreement with theory leaves no doubt that we are creating large numbers of weakly bound molecules. These highly vibrationally excited molecules could be used to study ultracold molecule–molecule, or molecule–atom, collisions[22,24,25]. Further, the explicit coupling of a quantum degenerate gas of fermionic atoms to bosonic molecules could possibly be developed as a method to facilitate creation of a predicted exotic fermionic superfluid. In addition, our molecule detection technique could be extended to measure the gap energy in this superfluid phase[26,27]. □

Received 29 April; accepted 19 May 2003; doi:10.1038/nature01738.

1. Wynar, R., Freeland, R. S., Han, D. J., Ryu, C. & Heinzen, D. J. Molecules in a Bose-Einstein condensate. *Science* **287,** 1016–1019 (2002).
2. Donley, E. A., Claussen, N. R., Thompson, S. T. & Wieman, C. E. Atom–molecule coherence in a Bose–Einstein condensate. *Nature* **417,** 529–533 (2002).
3. Holland, M., Kokkelmans, S. J. J. M. F., Chiofalo, M. L. & Walser, R. Resonance superfluidity in a quantum degenerate Fermi gas. *Phys Rev. Lett.* **87,** 120406 (2001).
4. Timmermans, E., Furuya, K., Milloni, P. W. & Kerman, A. K. Prospect of creating a composite Fermi-Bose superfluid. *Phys. Lett. A* **285,** 228–233 (2001).
5. Feshbach, H. A unified theory of nuclear reactions. *II. Ann. Phys. (NY)* **19,** 287–313 (1962).
6. Stwalley, W. C. Stability of spin-aligned hydrogen at low temperatures and high magnetic fields: New field-dependent scattering resonances and predissociations. *Phys. Rev. Lett.* **37,** 1628–1631 (1976).
7. Tiesinga, E., Verhaar, B. J. & Stoof, H. T. C. Threshold and resonance phenomena in ultracold ground-state collisions. *Phys. Rev. A* **47,** 4114–4122 (1993).
8. Inouye, S. *et al.* Observation of Feshbach resonances in a Bose–Einstein condensate. *Nature* **392,** 151–154 (1998).
9. Cornish, S. L., Claussen, N. R., Roberts, J. L., Cornell, E. A. & Wieman, C. E. Stable ^{85}Rb Bose-Einstein condensates with widely tunable interactions. *Phys. Rev. Lett.* **85,** 1795–1798 (2000).
10. Loftus, T., Regal, C. A., Ticknor, C., Bohn, J. L. & Jin, D. S. Resonance control of elastic collisions in an optically trapped Fermi gas of atoms. *Phys. Rev. Lett.* **88,** 173201 (2002).
11. Dieckmann, K. *et al.* Decay of an ultracold fermionic lithium gas near a Feshbach resonance. *Phys. Rev. Lett.* **89,** 203201 (2002).
12. O'Hara, K. M. *et al.* Measurement of the zero crossing in a Feshbach resonance of fermionic ^{6}Li. *Phys. Rev. A* **66,** 041401 (2002).
13. Regal, C. A., Ticknor, C., Bohn, J. L. & Jin, D. S. Tuning p-wave interactions in an ultracold Fermi gas of atoms. *Phys. Rev. Lett.* **90,** 053201 (2003).
14. O'Hara, K. M., Hemmer, S. L., Gehm, M. E., Granade, S. R. & Thomas, J. E. Observation of a strongly interacting degenerate Fermi gas of atoms. *Science* **298,** 2179–2182 (2002).
15. Regal, C. A. & Jin, D. S. Measurement of positive and negative scattering lengths in a Fermi gas of atoms. *Phys. Rev. Lett.* (in the press).
16. Bourdel, T. *et al.* Measurement of interactions energy near a Feshbach resonance in a ^{6}Li Fermi gas. Preprint at ⟨http://arXiv.org/cond-mat/0303079⟩ (2003).
17. Timmermans, E., Tommasini, P., Hussein, M. & Kerman, A. Feshbach resonances in atomic Bose-Einstein condensates. *Phys. Rep.* **315,** 199–230 (1999).
18. Abeelen, F. A. & Verhaar, B. J. Time-dependent Feshbach resonance scattering and anomalous decay of a Na Bose-Einstein condensate. *Phys. Rev. Lett.* **83,** 1550–1553 (1999).
19. Mies, F. H., Tiesinga, E. & Julienne, P. S. Manipulation of Feshbach resonance in ultracold atomic collisions using time-dependent magnetic fields. *Phys. Rev. A* **61,** 022721 (2000).
20. Stenger, J. *et al.* Strongly enhanced inelastic collisions in a Bose-Einstein condensate near Feshbach resonances. *Phys. Rev. Lett.* **82,** 2422–2425 (1999).
21. DeMarco, B. & Jin, D. S. Onset of Fermi degeneracy in a trapped atomic gas. *Science* **285,** 1703–1706 (1999).
22. Soldán, P., Cvitas, M. T., Hutson, J. M., Honvault, P. & Launay, J.-M. Quantum dynamics of ultracold Na + Na_2 collisions. *Phys. Rev. Lett.* **89,** 153201 (2002).
23. Ratcliff, L. B., Fish, J. L. & Konowalow, D. D. Electronic transition dipole moment functions for transitions among the twenty-six lowest-lying states of Li_2. *J. Mol. Spectrosc.* **122,** 293–312 (1987).
24. Balakrishnan, N., Forrey, R. C. & Dalgarno, A. Quenching of H_2 vibrations in ultracold ^{3}He and ^{4}He collisions. *Phys. Rev. Lett.* **80,** 3224–3227 (1998).
25. Forrey, R. C., Balakrisnan, N., Dalgarno, A., Haggerty, M. R. & Heller, E. J. Quasiresonant energy transfer in ultracold atom-diatom collisions. *Phys. Rev. Lett.* **82,** 2657–2660 (1999).
26. Petrosyan, K. G. Fermionic atom laser. *JETP Lett.* **70,** 11–16 (1999).
27. Torma, P. & Zoller, P. Laser probing of atomic Cooper pairs. *Phys. Rev. Lett.* **85,** 487–490 (2000).

Acknowledgements We thank E. A. Cornell, C. E. Wieman, C. H. Greene and S. Inouye for discussions. This work was supported by the NSF and NIST; C.A.R. acknowledges support from the Hertz Foundation.

Competing interests statement The authors declare that they have no competing financial interests.

Correspondence and requests for materials should be addressed to C.A.R. (regal@jilau1.colorado.edu).

Achromatic Fresnel optics for wideband extreme-ultraviolet and X-ray imaging

Yuxin Wang*, Wenbing Yun* & Chris Jacobsen*†

** Xradia, Inc., 4075A Sprig Drive, Concord, California 94520, USA*
† Department of Physics & Astronomy, Stony Brook University, Stony Brook, New York 11794, USA

Advances in extreme-ultraviolet (EUV) and X-ray optics are providing powerful new capabilities in high-resolution imaging and trace-element analysis of microscopic specimens[1], and the potential for fabricating devices of smaller critical dimensions in next-generation integrated circuit lithography[2]. However, achieving the highest resolution with such optics usually requires the illuminating EUV or X-ray beam to be highly monochromatic. It would therefore be highly desirable to have large-field-of-view, sub-100-nm resolution optics that are achromatic to a significant degree, allowing more light to be utilized from broader bandwidth sources such as laser-produced plasmas. Here we report an achromatic Fresnel optical system for EUV or X-ray radiation that combines a Fresnel zone plate with a refractive lens with opposite chromatic aberration. We use the large anomalous dispersion property of the refractive lens material near an absorption edge to make its fabrication practical. The resulting structure can deliver a resolution comparable to that of the Fresnel zone plates that have achieved the highest resolution (25 nm; ref. 3) in the entire electromagnetic spectrum, but with an improvement of two or more orders of magnitude in spectral bandwidth.

When Röntgen discovered X-rays in 1895, he immediately searched for a means to focus them[4,5]. On the basis of uncertain observations of slight refraction in prisms, he stated that the index of refraction for X-rays in materials must be no more than about $n = 1.05$ if it differed at all from unity. Two decades later, Einstein[6] proposed that the refractive index for X-rays was $n = 1 - \delta$ with $\delta \approx 10^{-6}$, allowing for total external reflection at grazing incidence angles satisfying $\cos\theta_c = 1 - \delta$, giving $\theta_c \approx \sqrt{2\delta}$ or of the order of 1 mrad (here θ_c is the critical angle). Modern measurements give critical angles of, for example, 9 mrad for 8.98-keV X-rays from gold surfaces; nonetheless, this sets a fundamental limit to the maximum numerical aperture, NA (and thus spatial resolution), of polychromatic X-ray focusing optics. While these optics have advanced from early demonstrations[7] to sub-500-nm focusing[8], demonstrated routes to higher spatial resolution EUV and X-ray imaging and lithography have instead involved optics for monochromatic radiation. Such optics include Fresnel zone plates[9] with 25-nm potential image resolution[3] and high efficiency; simple[10], Fresnel[11], and compound[12] refractive lenses with spatial resolution to about 200 nm (ref. 13); and mirror optics coated with synthetic multilayers[14] which have achieved 50-nm resolution in lithography applications[15]. These approaches have led to significant advances in EUV and X-ray science.

However, all of these higher-resolution methods require the illuminating EUV or X-ray beam to be highly monochromatic. For certain experiments, such as absorption spectroscopy with focused, monochromatized X-ray beams, the demands of these optics for narrow spectral bandwidth illumination are easily met without compromising experimental throughput. With broader-bandwidth EUV or X-ray sources, such as laser-produced plasmas and line emission from X-ray targets, the availability of achromatic optics would allow significantly more light to be utilized for experiments and applications.

